Computers and Geotechnics 134 (2021) 104103

Contents lists available at ScienceDirect

Computers and Geotechnics

journal homepage: www.elsevier.com/locate/compgeo

Research Paper

Soil-structure interaction of surface footings

Cristiano Garbellini *, Lyesse Laloui

Swiss Federal Institute of Technology, EPFL, Laboratory of Soil Mechanics, EPFL-ENAC-IIC-LMS, Station 18, CH-1015 Lausanne, Switzerland

ARTICLE INFO

Keywords:
Bearing capacity
Concrete cracking
Stress field
Strut-and-tie model
Theory of plasticity
Upper and lower bounds

ABSTRACT

Limit-state analysis of soil-structure interacting systems is a classical problem in theoretical and applied soil mechanics. Usually, the capacities of both components are evaluated separately. However, it is well known that soil-structure interaction plays a major role in the actual behaviour at failure of such systems. Despite the complexity of a rigorous mathematical treatment of the problem, the limit theorems of the theory of plasticity and appropriate consideration of the failure modes of the structural element allow to address soil-structure interaction in a simplified manner. This study shows how the existing solutions for the bearing pressure and footing structural resistance can be coupled to evaluate the impact of the soil-structure interaction. Further, lower and upper bound solutions are developed for foundations that have a slender cross-section.

1. Introduction

Solutions to limit-state problems from the point of view of soil mechanics generally consider the structural component as a rigid or perfectly flexible body, with a focus on the constitutive modelling of the interface and the soil (Rankine, 1857; Golder, 1942; Terzaghi, 1943; Meyerhof, 1951; Lundgren and Mortensen, 1953; Meyerhof, 1955; de Beer, 1970; Martin, 2005a; Zhu and Michalowski, 2005; Loukidis and Salgado, 2009). By contrast, the approach of structural mechanics focuses primarily on the identification of structural failure modes for members subjected to simplified loading conditions (e.g. uniform, triangular) (Campana and Muttoni, 2010; Pérez Caldentey et al., 2012; Campana et al., 2014; Simões et al., 2016; Simões et al., 2016).

Evidently, these simplifications are useful to limit the number of involved parameters and control the governing failure mechanisms in laboratory testing. However, little effort is made in attempting to combine the respective outcomes within a unified framework.

Recently, rigorous limit-state solutions of soil-structure systems were presented for surface footings and cut-and-cover tunnels (de Buhan, 2007; Plumey, 2007). These solutions consider the possibility of simultaneous failure within the structure and the soil, showing the great impact of mutual interactions on the actual performance of such systems.

With the availability of modern software for limit analysis, e.g. (Limit State Ltd, 2019; Optum Computational Engineering, 2019), similar solutions can be directly obtained in many cases. However, analytical or semi-analytical solutions are fundamental to assess the validity of those results. They are useful also because structural failure modes sometimes fall outside the applicability of the theory of plasticity, e.g. shear failure of slender concrete beams without transverse reinforcement. These modes cannot be captured by the aforementioned software for limit analysis and missing one of such failure modes might lead to catastrophic consequences.

In this study, surface footings under centred vertical load were examined as a reference case. An attempt was made to define a unified framework for the analysis of the collapse load considering soil-structure interaction in a simplified manner. For this purpose, sections two to four review the main concepts of soil bearing capacity, contact pressure distribution, and shear capacity of concrete members without transverse reinforcement. The fifth section is dedicated to the soil-structure interaction. It is shown that the knowledge of the three above-mentioned aspects can be combined in a useful way to obtain both quantitative and qualitative outcomes on the overall ultimate state of the foundation. New lower and upper bound solutions for combined failure were derived and extended to the three-dimensional case.

It is believed that, apart from establishing a unified approach toward a more rational limit-state analysis for soil-structure interacting systems, this study might help in soil and structural mechanics education.

2. Current practice for surface footings collapse analysis

2.1. Bearing capacity of soils

The maximum load, eventually expressed as average pressure, that a

* Corresponding author.
E-mail address: cristiano.garbellini@gmail.com (C. Garbellini).

https://doi.org/10.1016/j.compgeo.2021.104103
Received 18 August 2020; Received in revised form 6 February 2021; Accepted 17 February 2021
Available online 21 March 2021

mass of soil can sustain without producing uncontrolled settlements or without causing catastrophic damages to the superstructure is termed *bearing capacity*. This definition follows the interpretation of the *collapse load* given by Hill (1951) and Drucker et al. (1951) in the framework of the theory of plasticity.

The type of failure of rigid footings resting on dense/compact soils ($\gamma > 20$ kN/m^3, γ: soil self-weight) is known as *general shear failure* (Terzaghi, 1943). This failure mechanism is depicted for strip footings in Fig. 1 (Lundgren and Mortensen, 1953). The plastically deformed soil is pushed outward and upward. Depending on the base roughness, footing breadth, and soil properties, a trapped elastic wedge might move downward as an extension of the footing (Lundgren and Mortensen, 1953; Davis and Booker, 1971, 1973).

The resistance of the soil is due to its apparent cohesion and the weight of displaced soil. In terms of average contact pressure $p_u = Q_u/B$, we can employ the classical Terzaghi's form (Terzaghi, 1943):

$$\frac{p_u}{c} = N_c + GN_\gamma \tag{1}$$

where c is the apparent cohesion; $G = 0.5\gamma B/c$ is the dimensionless soil weight parameter (Cox, 1962), with B denoting the footing breadth, and N_c and N_γ the bearing capacity coefficients. For a weightless general soil or a purely cohesive soil, the exact value of N_c is given by the Prandtl solution (Prandtl, 1920):

$$N_c = \cot\phi(e^{\pi\tan\phi}N_\phi - 1) \tag{2}$$

where $N_\phi = \tan^2(\pi/4 + \phi/2)$ is the flow value (Terzaghi, 1943), whereas for a cohesionless soil the exact value of N_γ is given by Martin (2004, 2005b), and can be estimated with good accuracy through the older relation proposed by Meyerhof (1961):

$$N_\gamma = (e^{\pi\tan\phi}N_\phi - 1)\tan(1.4\phi) \tag{3}$$

The exact solution for a general soil, p_u/c, can be obtained with the software ABC (Martin, 2004).

Solutions for rectangular footings were obtained empirically (Terzaghi, 1943; Meyerhof, 1951; Skempton, 1951; de Beer, 1970), with the limit equilibrium or limit analysis method (Meyerhof, 1951; Shield and Drucker, 1953; Shield, 1955; Michalowski, 2001; Salgado et al., 2004; Lyamin et al., 2007), and through incremental elastic–plastic constitutive laws (Michalowski and Dawson, 2002; Zhu and Michalowski, 2005; Gourvenec et al., 2006). They are generally expressed through shape factors that multiply the solution for strip footings. Experiments showed that, for a given footing breadth, the bearing capacity p_u increases with an increasing aspect ratio B/L for saturated undrained clays (Skempton, 1942; Skempton, 1951), and decreases with an increasing aspect ratio for dry sands (Meyerhof, 1948; Meyerhof, 1951; Hansen, 1961; de Beer, 1961, 1970).

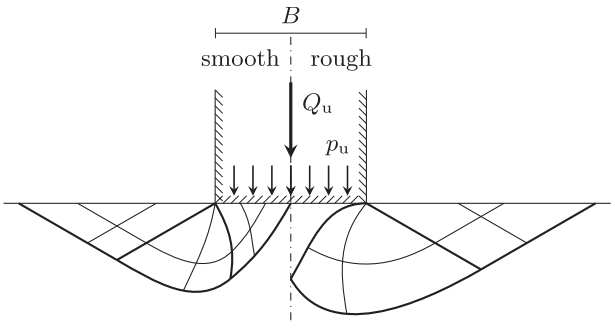

Fig. 1. Failure mechanism of smooth and rough strip footings resting on a dense and compact soil.

2.2. Contact pressure

The contact pressure distribution under a surface footing subjected to a centred vertical load is mainly a function of the footing rigidity, soil stiffness, and soil shear strength properties. A qualitative representation of pressure distribution for strip foundations is shown in Fig. 2. For comparison, the distribution over an elastic half-space is also drawn.

In a purely cohesive soil, the contact pressure at failure is uniform under strip footings and increases slightly toward the footing centre under circular and rectangular footings (Hencky, 1923; Meyerhof, 1951; Shield, 1955).

In a cohesionless soil, the shear strength at the footing edge is zero (unconfined soil element) and increases toward the footing centre. Therefore, the ultimate contact pressure follows a similar trend. The shape varies between triangular, parabolic, and ellipsoidal depending on the soil characteristics, and footing roughness and breadth (Terzaghi, 1943; Taylor, 1948; Meyerhof, 1951; Smith, 2005; Loukidis et al., 2008; Saran, 2017).

In a general cohesive frictional soil, the final distribution is a combination of the former. Whether it is closer to that of a purely cohesive or a cohesionless soil, it will depend on the parameters G and ϕ.

2.3. Shear capacity of concrete members without transverse reinforcement

The behaviour of a footing cross-section can be analysed through the theory for concrete members without transverse reinforcement. One-way shear resistance of concrete members without transverse reinforcement is affected by load distribution and slenderness. This is usually displayed with the help of the so-called Kani's valley (Kani, 1964), where the shear capacity is plotted against the shear span ratio $\alpha = a/d$ (a: shear span, d: effective depth; cf. Fig. 3). This diagram identifies different regimes of shear carrying actions (Fernández Ruiz et al., 2015). The direct strut action governs deep beams ($\alpha < \alpha_1 \approx 1$) and the member can be analysed with the strut-and-tie or stress fields method (Marti, 1985; Schlaich et al., 1987). In short span beams ($\alpha_1 < \alpha < \alpha_2 \approx 2.5-3$), the development of a critical crack within the compressive strut may limit the shear capacity. The modified stress fields theory (Vecchio and Collins, 1986), which accounts for the reduction of concrete compressive strength due to the transverse tensile strain, can be used to analyse these structural elements (Fernández Ruiz et al., 2015). The shear resistance of slender beams ($\alpha_2 < \alpha < \alpha_3 \approx 5-8$) is affected by both strain and size effects (Bazant and Kim, 1984; Muttoni and Schwartz, 1991). The critical shear crack

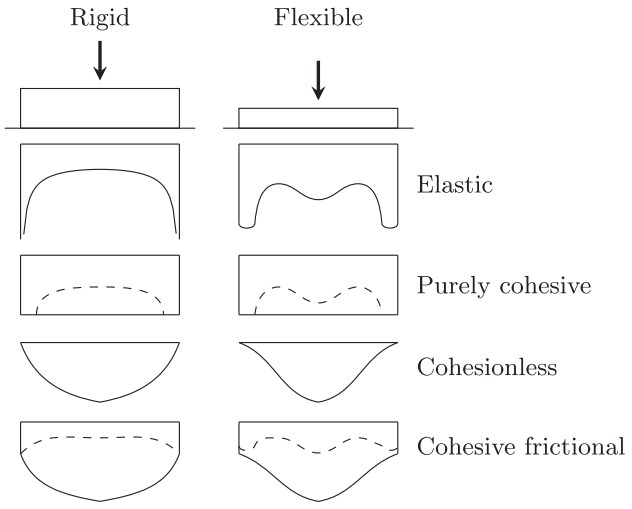

Fig. 2. Qualitative contact pressure distribution under isolated surface strip footings. Solid lines represent the distribution at failure, whereas dashed lines correspond to a state prior to collapse.

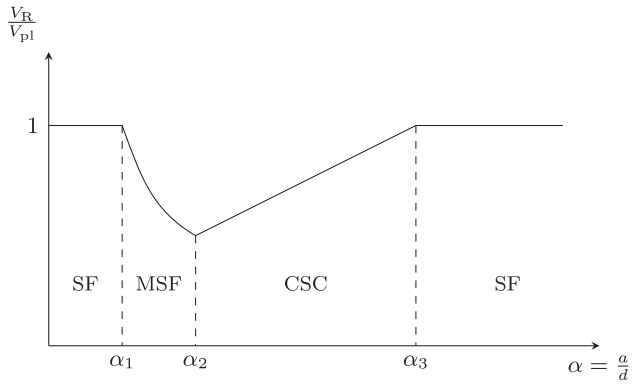

Fig. 3. Relative shear capacity versus shear span ratio. V_R is the shear resistance, V_{pl} denotes the shear force that causes the yielding of the flexural reinforcement and crushing of the concrete, a stands for the shear span, and d is the effective depth (maximum effective depth in a variable depth footing). The design method for each regime is indicated: SF stands for stress fields, MSF stands for modified stress fields, and CSC stands for critical shear crack theory.

theory consistently accounts for both phenomena (Muttoni and Fernández Ruiz, 2008; Fernández Ruiz et al., 2015; Cavagnis et al., 2018). For larger values of slenderness ($\alpha > \alpha_3$), the bending resistance is the governing factor, and the classical Euler–Bernoulli beam theory can be employed (Schlaich et al., 1987; Pérez Caldentey et al., 2012).

3. Effects of soil-structure interactions

Based on the previous sections, it is clear that soil-structure interaction plays a major role on the actual behaviour at failure of foundations. In this regard, a series of considerations can be drawn that either allow to take directly into account soil-structure interaction or help make decisions related to a higher level of performance. These considerations are presented in the following subsections.

3.1. Deep beams

Squat footings pertaining to the category of deep beams can generally be considered rigid. Flexural cracking is limited and barely penetrates within the compression field. These types of elements can be analysed without loss of accuracy with a simple strut-and-tie model by replacing the contact pressure with two equivalent concentrated loads acting at a quarter of the footing breadth (Schlaich et al., 1987; Kostic, 2009) (uniform contact pressure). A proper consideration of the contact pressure distribution has little influence on the magnitude of the bearing capacity owing to the small value of the ratio B/d.

In this case, the analysis is straightforward. The inclination of the direct strut with respect to the horizontal is expressed as follows:

$$\tan\theta_c = 4\frac{d - 0.5x_c}{B - b} \approx 4\frac{d - 0.5x_c}{B} \tag{4}$$

where x_c is the depth of the plastically compressed concrete. The force carried by the strut when the soil bearing capacity is fully mobilised is given by the following expression:

$$C = \frac{B}{2\sin\theta_c} p_u \tag{5}$$

3.2. Short span beams

In footings characterised by a short span beam cross-section, flexural cracks may penetrate within the compression field transversely and reduce the concrete compressive strength. The theory of plasticity can be applied if a strength reduction factor that accounts for the transverse tensile strain is introduced (Vecchio and Collins, 1986; Muttoni et al., 1996; Muttoni et al., 2011):

$$f_{ce} = k_c f_{cp} \tag{6}$$

where f_{ce} is the effective concrete compressive strength, f_{cp} is the concrete equivalent plastic strength, and k_c is the reduction factor.

The influence of the pressure distribution increases with respect to the previous case and replacement with two concentrated loads is a very rough approximation. This is mainly due to the fact that k_c evaluated at the location of the resultant strut is not a representative mean value of the whole compression field.

As an example, the collapse load of a footing subjected to different pressure distributions was computed with the finite element software jconc (Fernández Ruiz and Muttoni, 2007), which is an automatic generator of plane stress elastic–plastic stress fields for reinforced concrete members. The footing had constant depth, breadth $B = 150$ cm, effective depth $d = 45$ cm, flexural reinforcement ratio $\rho = 1.12\%$, concrete compressive strength $f_{cp} = 30$ MPa, null concrete tensile strength $f_{ct} = 0$, concrete Young's modulus $E_c = 30$ GPa, steel yield stress $f_y = 500$ MPa, and steel Young's modulus $E_s = 205$ GPa. Three pressure distributions were considered: (a) uniform, (b) triangular, and (c) external triangular, i.e. the pressure is zero at the footing centre and increases linearly toward the footing edges. Distribution (c) is not realistic, but it is useful to appreciate the influence of the strain effect. The results are shown in Fig. 4. Taking the collapse load of case (a) as a reference, its value increased by 48.9 % for case (b) and decreased by 17.9% for case (c). Considering that the actual contact pressure distribution when the soil bearing capacity is reached is between case (a) and (b), its impact is considerable.

Therefore, the analysis of short span footings by means of strut-and-tie models should be performed with a refinement of the equivalent concentrated load distribution, which replaces the contact pressure. Simplified methods such as those proposed in (Davis and Selvadurai, 1996; Saran, 2017) might be used to redistribute the contact pressure more conveniently. In particular, the technique suggested in (Saran, 2017) allows to consider lower load levels than the soil bearing capacity.

Note that the assumption of uniform pressure is not on the safe side for highly cohesive and stiff soils loaded below their bearing capacity, because the contact pressure is minimum at the footing centre and maximum at the edges.

3.3. Slender beams

In Fig. 5, a generic slender footing subjected to a centred vertical load and uniform contact pressure shows the shear transfer mechanisms with the help of a strut-and-tie model (Pérez Caldentey et al., 2012). The total shear capacity is given by the following expression:

$$V_R = V_{dir} + V_{chord} + V_c \tag{7}$$

where V_{dir} is the contribution of the direct strut action, V_{chord} is the vertical component of the inclined compression chord, and V_c is the shear force that can be transferred across the critical shear crack.

It is evident that the contact pressure distribution can have a considerable impact on the shear resistance, and thus on the overall bearing capacity as well. Experiments carried out on slender cantilever beams confirmed this point (Pérez Caldentey et al., 2012). Note that for constant depth members, the shear capacity can be as high as 80 % for triangular loading compared to uniformly distributed loading. For the latter, the inclination of the compression chord can lead to an increase of the shear force up to 30 % (Stefanou, 1983; Pérez Caldentey et al., 2012).

When the shear span ratio of the footing cross-section is between α_1 and α_2, the foundation fails in shear by development of a critical crack. In this case, the member cannot be analysed by simply considering an equivalent homogeneous material characterised by a reduced compressive strength; the shear carrying mechanisms across the critical

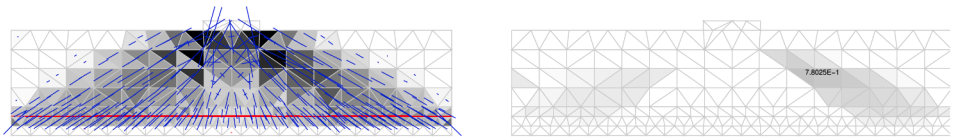

(a) Uniform contact pressure: $Q_u = 8.4\,\mathrm{MN}$, $k_{c,min} = 0.78$.

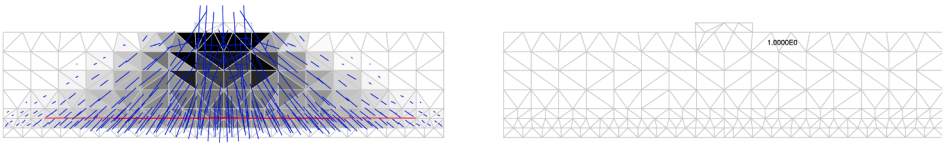

(b) Triangular contact pressure: $Q_u = 12.5\,\mathrm{MN}$, $k_{c,min} = 1$.

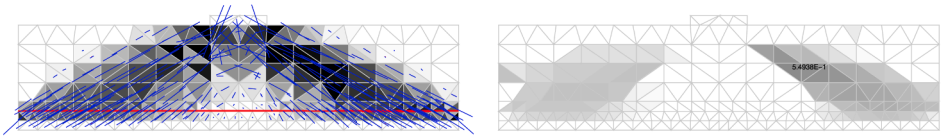

Fig. 4. Elastic–plastic stress field (left column) and k_c-value distribution (right column) at collapse for different contact pressure distributions.

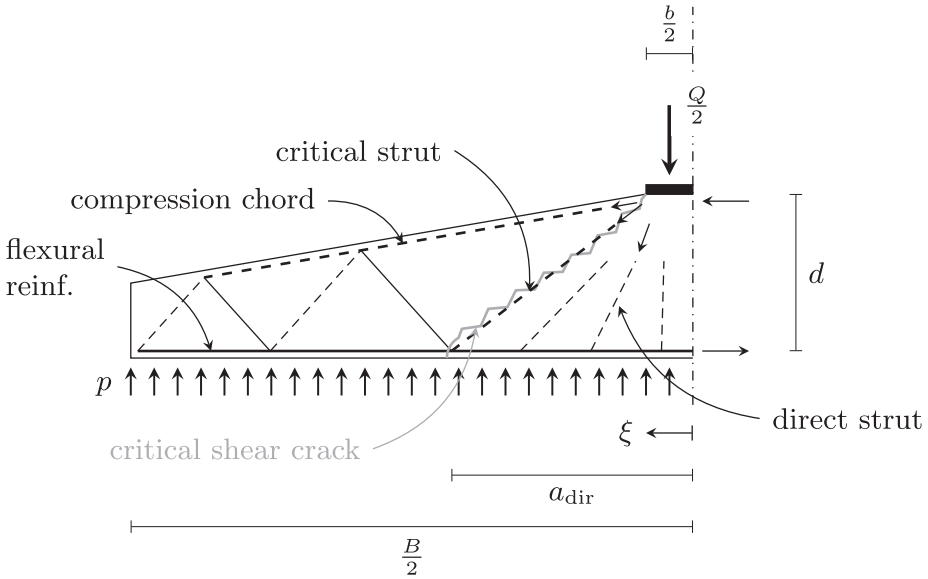

Fig. 5. Half of a slender footing with flexural reinforcement subjected to centred vertical load and uniform contact pressure. A strut-and-tie model (strut in dashed line and tie in solid line) shows the load transfer mechanisms. The critical shear crack is represented in grey. Adapted from (Pérez Caldentey et al., 2012).

crack must be explicitly taken into account.

An experimental study on cantilever beams (Pérez Caldentey et al., 2012) showed that the load over the region a_{dir} (Fig. 5), i.e. between the support and the section where the crack intercepts the flexural reinforcement, is carried by direct strut action. It was suggested that $a_{dir} \approx 2.75d + b/2$. Another experimental investigation (Cavagnis et al., 2015) revealed that this distance can fall in the range $d + b/2 \leqslant a_{dir} \leqslant 2.6d + b/2$. Thus, the shear force that must be transmitted through the critical shear crack is expressed as follows (cf. Fig. 5):

$$V_{E,c} = \int_{B/2}^{a_{dir}} p(\xi)\,\mathrm{d}\xi - V_{chord}(\xi = a_{dir}) \tag{8}$$

According to the critical shear crack theory, the shear capacity across the crack V_c is a function of the crack opening and roughness. The former is then supposed proportional to the strain evaluated at a specific critical section times the effective depth, and the latter can be expressed through the aggregate size. The failure criterion is a hyperbolic law (Muttoni and Fernández Ruiz, 2008):

$$\frac{V_c}{1[\mathrm{m}]d\sqrt{f_{ck}}} = \frac{1/3}{1 + 120\,\epsilon d/d_{dg}} \qquad (\text{SI units}: \ \mathrm{MPa}, \mathrm{mm}) \tag{9}$$

where f_{ck} is the characteristic compressive cylinder strength of concrete; ϵ denotes the strain evaluated in the critical section at $0.6d$ from the outermost compressed fibre, assuming plane-deformed sections and linear elastic behaviour of concrete in compression (the tensile strength is neglected); $d_{dg} = 16\,\mathrm{mm} + d_g$ with d_g denoting the maximum aggregate size. The critical section is located at $d/2$ from the edge of the wall stressing the footing ($\xi_{cs} = b/2 + d/2$) and $a_{dir} = 2.75d + b/2$ (Pérez Caldentey et al., 2012).

Recently, a power-law failure criterion was proposed to improve the accuracy at low strain (Cavagnis et al., 2018):

$$\frac{V_c}{1[\mathrm{m}]d\sqrt{f_{ck}}} = \frac{k}{\sqrt{\epsilon_s d/d_{dg}}} \qquad (\text{SI units : MPa, mm}) \tag{10}$$

where k is a constant that depends on the main mechanical and geometrical parameters (e.g. $k = 0.019$ for simply supported beams subjected to point load and $k = 0.016$ for simply supported beams subjected to distributed loading (Cavagnis, 2017)), ϵ_s is the strain in the flexural reinforcement at the location of the critical section, and $d_{dg} = \min\{40\ \mathrm{mm}, 16\ \mathrm{mm} + d_g\}$. In the case of cantilever beams, the critical section is located at a distance d from the axis of the support ($\xi_{cs} = d$) and it is assumed that $a_{dir} = d$. Owing to the application of the load on the tension face, a_{dir} might be extended (Cavagnis, 2017) (increased dowel action):

$$\begin{aligned} \Delta a_{dir} &= 0.2\left(\frac{B}{2} - a_{dir}\right) = 0.1B - 0.2d \\ a_{dir,tot} &= 0.1B + 0.8d \end{aligned} \tag{11}$$

Eqs. (9) and (10), shown graphically in Fig. 6, are related through the approximate relation $\epsilon \approx 0.41\epsilon_s$ (Muttoni and Fernández Ruiz, 2008).

Adopting reasonable assumptions and assuming typical reinforcement and partial safety factors employed in Switzerland (Muttoni and Fernández Ruiz, 2008), the hyperbolic law (9) leads to the following design formula:

$$\frac{V_{cd}}{1[\mathrm{m}]d\sqrt{f_{ck}}} = \frac{0.2}{1 + 0.0022d\frac{M_{Ed}}{M_{Rd}}} \qquad (\text{SI units : MPa, mm}) \tag{12}$$

where M_{Ed} and M_{Rd} are the design values of the acting bending moment and resisting bending moment, respectively, at the critical section. Similarly, a closed-form expression was obtained from the power law (10) (Cavagnis, 2017):

$$\frac{V_{cd}}{1[\mathrm{m}]d} = \frac{\kappa}{\gamma_c}\left(\rho f_{ck}\frac{d_{dg}}{a_{cs}}\right)^{1/3} \qquad (\text{SI units : MPa, mm}) \tag{13}$$

where γ_c denotes the partial safety factor for concrete strength (1.5 according to the Swiss code (SIA, 2013)), $a_{cs} = M_{Ed}/V_{Ed}$ is the moment-to-shear ratio at the critical section, and κ is a parameter equivalent to k in (10). In the case of cantilever beams, κ takes the following form:

$$\kappa = \frac{1}{1 - 0.15}(0.5 + 0.2\alpha_{cs}^{1/3}) \tag{14}$$

with $\alpha_{cs} = a_{cs}/d$.

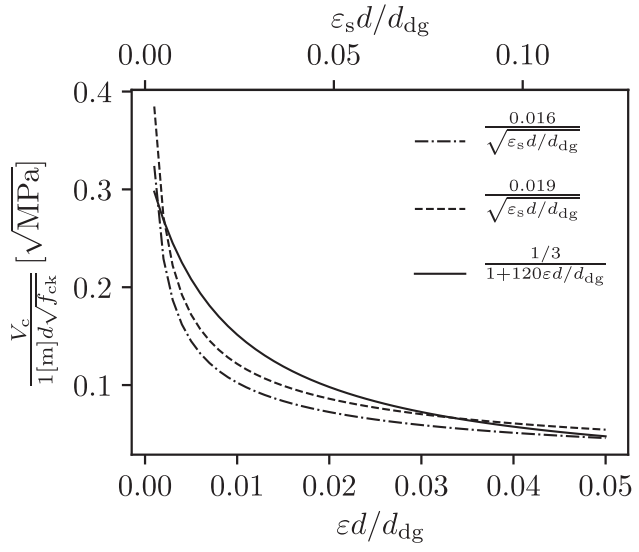

Fig. 6. Shear failure criteria based on the critical shear crack theory.

Note that in both code-like equations, the location of the critical section was mainly calibrated against beams subjected to point or uniformly distributed loading. However, it was shown that such a location is also representative for triangular loading (Pérez Caldentey et al., 2012). Therefore, it is reasonable to assume that it remains representative for general loading conditions, whereas the actual degree of accuracy remains unknown.

Given that the structural resistance is governed by the shear capacity of the critical crack V_c, and that the latter and the acting shear force $V_{E,c}$ are affected by the loading conditions, the actual performance of these foundations is largely influenced by soil-structure interaction. Despite the theoretical exact contact pressure distribution is generally difficult to assess, it can be approximated by simple shapes (rectangular, triangular, parabolic, ellipsoidal, and trapezoidal), as mentioned above. Accordingly, a_{cs} may take the expressions given in Table 1.

The shear capacity of the critical shear crack relative to the case of uniform contact pressure $V_c/V_{c,rect}$ is plotted, according to the closed-form Eq. (13), against the moment-to-shear slenderness ratio $\alpha_{cs,rect}$ in Fig. 7. The increase of V_c is maximum for the triangular distribution, reaching approximately 9 % to 10 %. Note that the actual increase of the structural bearing capacity V_R is enhanced by the reduction of the shear force $V_{E,c}$, which has to be transferred across the critical crack, and the increase of the direct strut action V_{dir}.

Therefore, the influence of soil-structure interaction can be estimated in a simplified manner with the help of Table 1. The resulting evaluation procedure is as follows:

- Check the soil average bearing capacity with (1)
- Define the pressure distribution
- Check the structural shear capacity V_c:
  - Compute $V_{E,c}$ with (8)
  - Compute a_{cs} with Table 1
  - Compute V_c either with (12) or with (13). If the former is used, compute the acting moment at the critical section as $M_{Ed} = a_{cs}\int_{B/2}^{\xi_{cs}} p(\xi)\,\mathrm{d}\xi$
- Check the direct strut capacity V_{dir}:
  - Compute $V_{dir} = \int_{a_{dir}}^{0} p(\xi)\,\mathrm{d}\xi$
  - Check the flexural reinforcement and concrete with a strut-and-tie or stress fields model, according to the theory for deep or short span beams

It should be emphasised that the shear resistance of the footing is affected by the strain level, which could be taken into account by adopting a contact pressure distribution that considers this aspect. Simplified contact pressure distributions as those proposed in this study that account for the strain level within the soil were proposed by (Saran, 2017).

In the case of surface rectangular footings, the above considerations hold only for the central region (in the length direction). Close to the end zones and for footings with high values of the aspect ratio B/L, i.e. close

Table 1
Expressions for the computation of $a_{cs} = M_{Ed}/V_{Ed}$. The value of ξ_{cs} is equal to $b/2 + d/2$ for the hyperbolic criterion and to d for the power law.

Pressure distribution	a_{cs}	$a_{cs}/a_{cs,rect}$
rectangular	$\frac{1}{2}(B/2 - \xi_{cs})$	1
triangular	$\frac{1}{3}(B/2 - \xi_{cs})$	0.67
parabolic	$\frac{3}{8}(B/2 - \xi_{cs})$	0.75
ellipsoidal	$\frac{4}{3\pi}(B/2 - \xi_{cs})$	0.85
trapezoidal	$\frac{1}{3}\frac{2\rho_p + 1}{\rho_p + 1}(B/2 - \xi_{cs})$[a]	$0.67\frac{2\rho_p + 1}{\rho_p + 1}$

[a] $\rho_p = p(\xi = B/2)/p(\xi = \xi_{cs})$

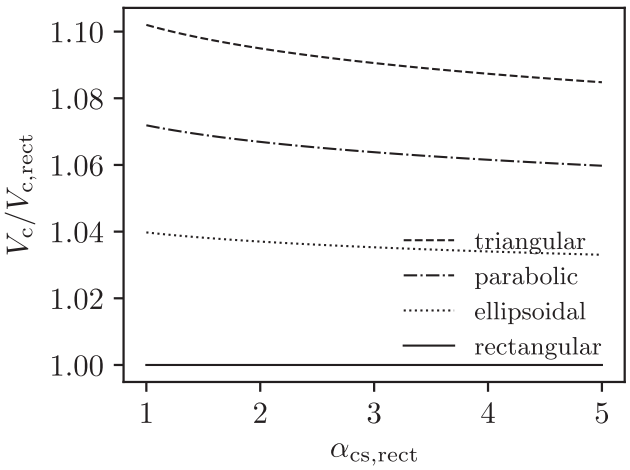

Fig. 7. Shear capacity of the critical shear crack V_c over the shear capacity of the critical shear crack for uniform pressure distribution $V_{c,rect}$, according to the closed-form Eq. (13), as a function of the moment-to-shear slenderness ratio $\alpha_{cs,rect} = a_{cs,rect}/d$.

to 1, three-dimensional effects on the contact pressure distribution become more important. In those situations, similar conclusions can be drawn, though they are not detailed here. In fact, there are no physical reasons to reject such conclusions. Actual values can be obtained by extending the suggested contact pressure shapes into three dimensions.

The above conclusions also apply qualitatively to concrete blocks loaded by a column. The governing structural failure is punching shear, which can be similarly investigated through the critical shear crack theory (Muttoni and Fernández Ruiz, 2008a; Muttoni et al., 2018).

3.4. Very slender beams

As the structural element becomes more deformable, the impact of the soil-structure interaction increases. In this section, outcomes obtained through the limit analysis method (Hill, 1951; Drucker et al., 1951, 1952) for footings with a very slender cross-section (cf. Fig. 3) are presented.

In the following, the soil is idealised as a perfectly rigid plastic isotropic homogeneous coaxial and associated continuum obeying the Tresca or Mohr–Coulomb yield condition. For simplicity, the terms Tresca/Mohr–Coulomb soil or material are used. The footing is a perfectly rigid plastic beam satisfying the normality condition in the space of generalised sectional stresses.

3.4.1. Plane strain problem

A combined failure mechanism for strip footings with limited flexural resistance was proposed by Plumey (Plumey et al., 2004; Plumey, 2007). The geometry of such rupture figure, symmetric with respect to the centre line, is shown in Fig. 8 for a purely cohesive soil (left-hand side) and for a general cohesive frictional soil (right-hand side). The kinematics is defined by the angular velocity ω and the corresponding centre of rotation, identified by the angle θ_0 and the distance x_0. The indentation of the footing causes the mass of soil between the ground surface and the failure line to rotate as a rigid body around the centre of rotation. Internal energy dissipation occurs along the lines of soil velocity discontinuity, in the footing plastic hinge, and eventually at the soil-footing interface. For purely cohesive soils, footing roughness is taken into account through an adherent behaviour, i.e. the interface is idealised as an infinitely thin layer of a Tresca material characterised by a shear yield strength βc, where $0 \leqslant \beta \leqslant 1$. For other soils, Coulomb interface friction characterised by the interface friction angle δ is assumed. The external power is due to the collapse load Q_u and the soil self-weight.

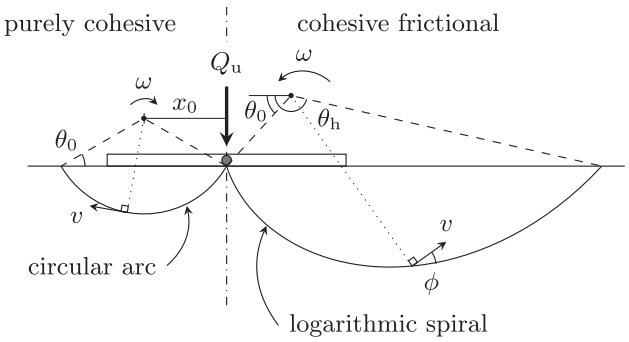

Fig. 8. Combined failure mechanism for plane strain conditions (Plumey, 2007). Velocity discontinuity lines within the soil are either a circular arc or a logarithmic spiral. The plastic hinge is shown with a grey circle in the middle. of the footing.

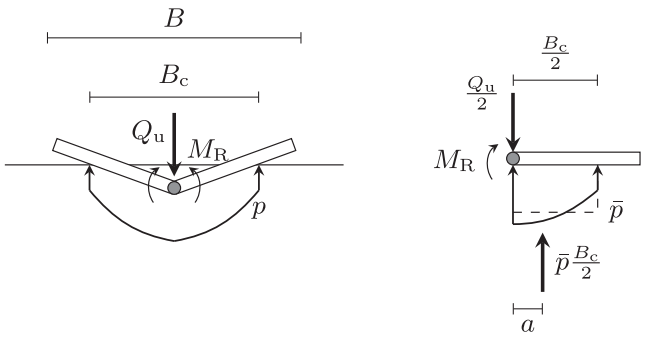

Fig. 9. Allowable stress field for combined failure in plane strain conditions (Plumey, 2007).

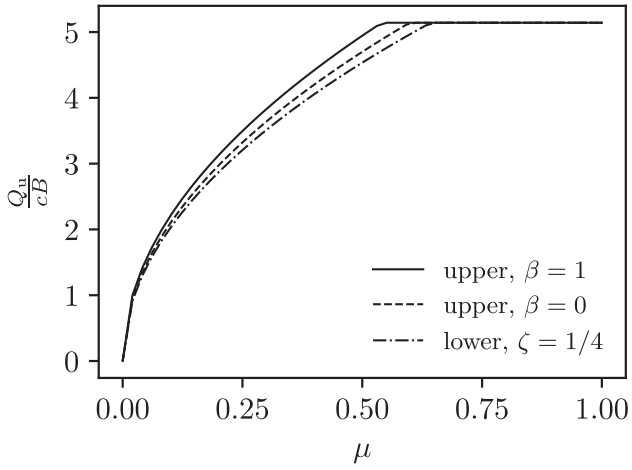

Fig. 10. Upper and lower bounds to the collapse load of a strip footing resting on a Tresca material. The normalised bearing capacity is plotted against the dimensionless resisting moment $\mu = M_R/(cB^2)$. The plateau corresponds to the well-known value $2 + \pi$.

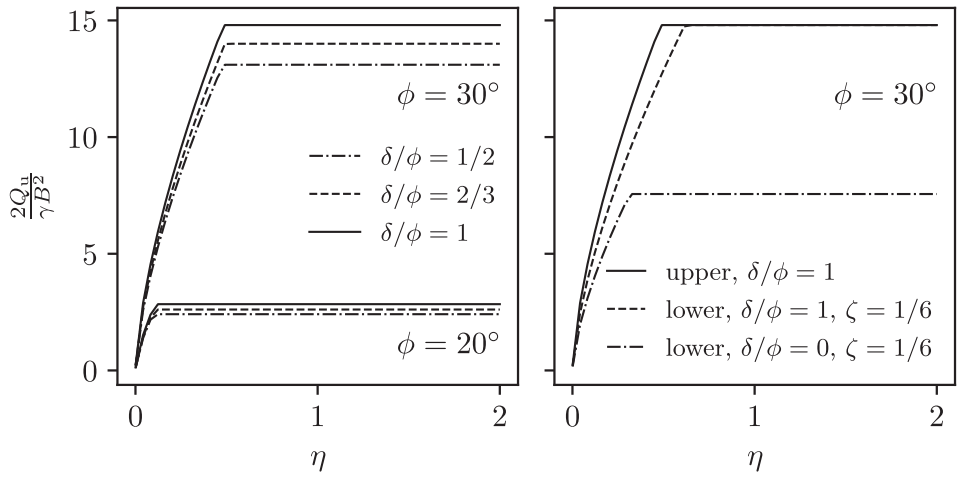

Fig. 11. Upper and lower bounds to the collapse load of a strip footing resting on a cohesionless Mohr–Coulomb material. Left-hand side: upper bounds; right-hand side: upper and lower bounds. The normalised bearing capacity is plotted against the dimensionless resisting moment $\eta = M_R/(\gamma B^3)$. The values of the general shear failure (plateau) are taken from Martin (2005b).

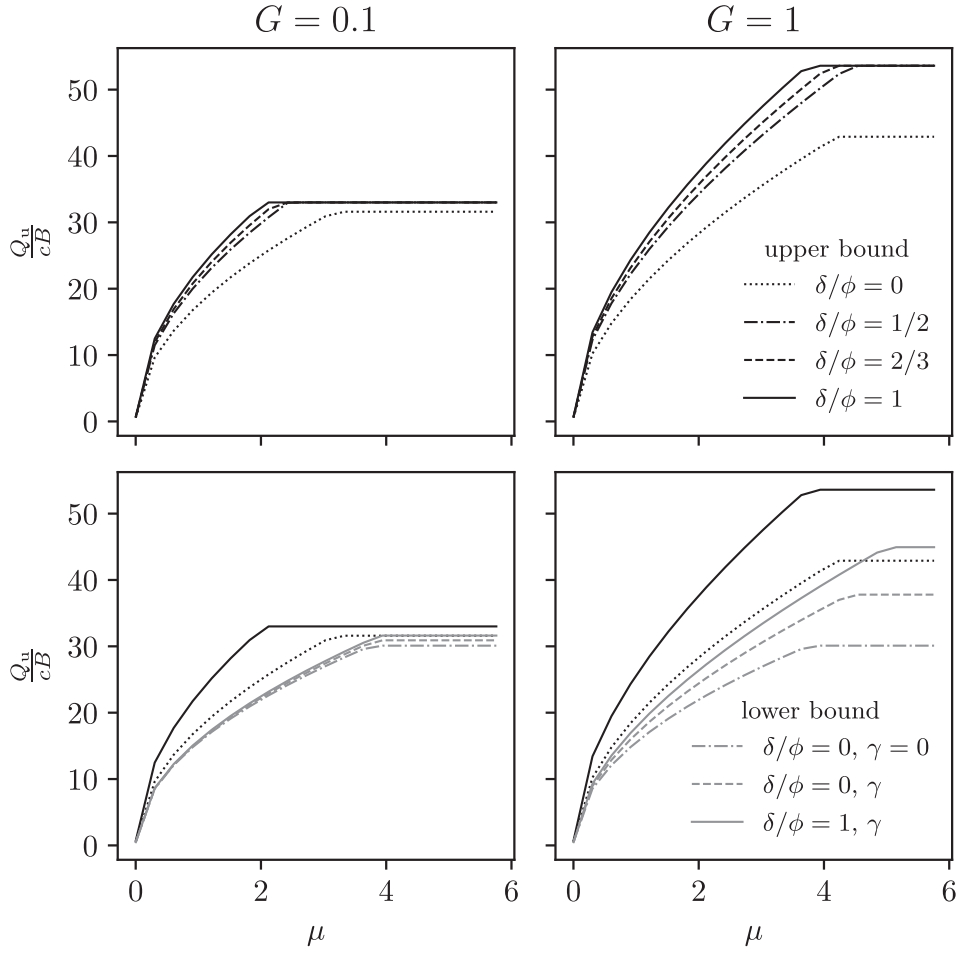

Fig. 12. Upper and lower bounds to the collapse load of a strip footing resting on a general Mohr–Coulomb material, $\phi = 30°$. First row: upper bounds; second row: black lines denote upper bounds whereas grey lines denote lower bounds.

Upper bounds were obtained by Plumey for Tresca and cohesionless Mohr–Coulomb soils,[1] (Plumey, 2007) (Fig. 10 and 11), and by the authors for a general Mohr–Coulomb soil (Garbellini and Laloui, 2018) (Fig. 12). The curves of the bearing capacity are characterised by an increasing branch, corresponding to the combined failure, and by a plateau, due to the general shear failure (rigid footing). Here, in contrast to (Plumey, 2007; Garbellini and Laloui, 2018), the plateau for the Mohr–Coulomb soils (sand and general soils) was taken from the complete solution given by Martin (2005a).

Note that the considered interface frictional behaviour for the upper bound solutions of the combined failure corresponds to a non-associated behaviour. However, the limit theorems are valid for frictional interfaces if the frictional forces are known, because they can be treated as surface tractions (Drucker and Prager, 1952; Drescher and Detournay, 1993). Given that the relative velocity at the interface is constant, and owing to the symmetry of the problem, the interface energy dissipation over half-footing is (Chen, 1975; Plumey, 2007; Garbellini and Laloui, 2018)

$$D_\delta = F_\mathrm{t}\,|v_\mathrm{t}| = \frac{Q_\mathrm{u}}{2}\tan\delta\,|v_\mathrm{t}| \tag{15}$$

where F_t is the resultant frictional force, δ the interface friction angle, and $|v_\mathrm{t}|$ the tangential relative velocity at the interface.

A lower bound was also derived by Plumey for the case of a Tresca material (Fig. 10). The admissible stress field was obtained by applying a contact pressure p, admissible for the soil, over a reduced contact breadth $B_\mathrm{c} \leqslant B$ (Fig. 9) such that $M(p, B_\mathrm{c}) \leqslant M_\mathrm{R}$. For the Tresca soil, such contact pressure is uniform and equal to $p_\mathrm{u} = cN_\mathrm{c} = c(2+\pi)$.

A general formula for the lower bound of any pressure distribution can be obtained by considering half of the footing, the average pressure due to the general shear failure p_u corresponding to a lower bound solution, the relative position of the resultant force of the actual contact pressure distribution $\zeta = a/B_\mathrm{c}$ (Fig. 9), and the contact breadth ratio $\zeta_\mathrm{c} = B_\mathrm{c}/B$. The solution can be expressed as follows:

$$\zeta_\mathrm{c} = \sqrt{\frac{2M_\mathrm{R}}{p_\mathrm{u}\zeta}} \leqslant 1 \tag{16a}$$

$$Q_\mathrm{u} = p_\mathrm{u}\zeta_\mathrm{c}B \tag{16b}$$

The procedure consists in computing p_u with (1), redistributing it in an admissible manner, e.g. with one of the simple shapes described in the previous section, and defining ζ (cf. Table 1).

For the Tresca material, considering $p_\mathrm{u} = cN_\mathrm{c} = c(2+\pi)$, the dimensionless resisting moment $\mu = M_\mathrm{R}/(cB^2)$, and $\zeta = 1/4$, leads to the result obtained by Plumey:

$$\frac{Q_\mathrm{u}}{cB} = \sqrt{8(2+\pi)\mu} \tag{17}$$

For a frictional soil, p_u is a function of the contact breadth (size effect). Introducing the dimensionless resisting moment $\eta = M_\mathrm{R}/(\gamma B^3)$, (16a) becomes, for a cohesionless Mohr–Coulomb material, as follows:

$$\zeta_\mathrm{c} = \left(\frac{4\eta}{N_\gamma\zeta}\right)^{1/3} \leqslant 1 \tag{18}$$

and the dimensionless bearing capacity is given by the following expression:

$$\frac{2Q_\mathrm{u}}{\gamma B^2} = \zeta_\mathrm{c}^2 N_\gamma \tag{19}$$

[1] The objective function of the combined failure mechanism for a cohesionless Mohr–Coulomb material was reviewed by the authors in view of a mistake in the derivation of the velocity field for the computation of the rate of energy dissipated at the soil-footing interface (Garbellini and Laloui, 2018).

The contact pressure distribution for smooth rigid footings is directly obtained with the method of stress characteristics (Larkin, 1968). It increases linearly from the footing edge to the centre. It was shown that the solution obtained in this way is complete (Martin, 2005a). Thus, a triangular distribution is a rigorous lower bound. Moreover, the triangular distribution corresponding to the smooth interface is a rigorous lower bound for any value of footing roughness according to the frictional limit theorems (Drucker, 1953). Improved lower bounds for rough bases can be obtained by considering the appropriate value of the bearing capacity factor N_γ. However, the distribution for rough footings cannot be obtained in the same way, owing to the presence of a non-plastic wedge beneath the base. Several authors suggested that the pressure distribution at collapse is parabolic (Terzaghi, 1943; Taylor, 1948; Smith, 2005; Loukidis et al., 2008) or can be well approximated by a triangular shape (Meyerhof, 1951; Kumar, 2003; Saran, 2017). If a triangular distribution is assumed, the solution for a cohesionless Mohr–Coulomb material is obtained with $\zeta = 1/6$ in (18) (Fig. 11), whereas for a parabolic distribution $\zeta = 3/16$ ($1/6 = 0.167$ and $3/16 = 0.188$).

Shield (1955) obtained a rigorous lower bound to the uniform normal strip load for a weightless general Mohr–Coulomb soil. The corresponding solution for the combined failure is shown at the bottom row of Fig. 12. The solution is obtained as in the case of a Tresca material, but with $N_\mathrm{c} = N_\mathrm{c}(\phi)$. Such solution is an absolute lower bound because base roughness and soil self-weight increase the soil bearing capacity.

For a ponderable Mohr–Coulomb material, the pressure at the instant of general shear failure is non-zero at the footing edge owing to the apparent cohesion, and then it increases in a linear or parabolic way toward the centre, as explained previously. Therefore, the computation of ζ requires the explicit knowledge of the contribution of the apparent cohesion and the soil self-weight to the bearing capacity, i.e. N_c and N_γ. However, when the principle of superposition is not adopted, such coefficients vary for each combination of ϕ and G, and the solution is generally given as the ratio p_u/c, or similarly, without specifying the individual contributions. Nevertheless, a lower bound solution can be obtained in a simple manner by using the superposition approach. It is known that the sum of the exact solutions of the collapse load of a purely cohesive soil and a cohesionless soil is a lower bound to the exact solution for the general Mohr–Coulomb soil (Terzaghi, 1943; Michalowski, 1997; Bolton and Lau, 1993)

$$N_\mathrm{c}(\phi, c, \gamma = 0) + GN_\gamma(\phi, c = 0, \gamma) \leqslant N_\mathrm{c}(\phi, c, \gamma) + GN_\gamma(\phi, c, \gamma) \tag{20}$$

where the bearing capacity factors are the exact ones. Owing to the fact that an exact solution is also a lower bound, it can be concluded that a lower bound estimate for a general soil can be obtained from the superposition approach and the two distinct exact solutions.

The improved lower bound for the combined failure can be obtained by independently computing ζ_c for a weightless cohesive frictional material (ζ_{cc}) and for a ponderable cohesionless frictional material ($\zeta_{c\gamma}$), and then taking the minimum. However, ζ_{cc} and $\zeta_{c\gamma}$ cannot be simply expressed as a function of the total resisting moment M_R, as before. This would not guarantee an admissible bending moment when the contributions are summed. To ensure an admissible bending moment, it is assumed that the weightless and cohesionless soils respectively contribute to the bending moment by M_c and M_γ as follows:

$$\begin{aligned} M_\mathrm{c} &= \rho_\mathrm{m} M_\mathrm{R} \\ M_\gamma &= (1-\rho_\mathrm{m}) M_\mathrm{R} \end{aligned} \tag{21}$$

Considering that $\mu = 2\eta G$ for a general soil, the contact breadth ratio is expressed as follows:

$$\begin{aligned}\zeta_c &= \min\{\zeta_{cc}, \zeta_{c\gamma}\}\\ \zeta_{cc} &= \left(\frac{2\rho_m\mu}{N_c\zeta}\right)^{1/2} \leqslant 1\\ \zeta_{c\gamma} &= \left(\frac{2(1-\rho_m)\mu}{GN_\gamma\zeta}\right)^{1/3} \leq 1\end{aligned} \tag{22}$$

and the dimensionless ultimate load is given by the following expression:

$$\frac{Q_u}{cB} = \zeta_c N_c + \zeta_c^2 G N_\gamma \tag{23}$$

The optimum is found by solving the following bounded maximisation problem:

$$\begin{aligned}&\max_{\rho_m} \frac{Q_u}{cB}\\ &0 \leqslant \rho_m \leqslant 1\end{aligned} \tag{24}$$

The problem was transformed in a minimisation problem by multiplying the objective function times -1. The L-BFGS-B algorithm (Byrd et al., 1995) implemented in SciPy (Virtanen et al., 2020) was used for the resolution. A triangular pressure distribution was considered for the soil-weight contribution. Some results are shown in Fig. 12 with grey lines. Note that the superposition approach, which considers interface friction and soil self-weight, provides a better lower bound, as expected.

3.4.2. Three-dimensional problem

A combined failure mechanism for footings with finite length subjected to a centred linear load can be obtained from that of a plane strain situation and considering an admissible velocity field (compatible and satisfying the normality condition) at the end faces.

The footing is now modelled as a rigid plate which develops a plastic hinge along its centre line (Fig. 13 and 15). The kinematics remains a plane strain motion and is similar to the bi-dimensional case.

The velocity field for a Tresca material is simply obtained by extending the bi-dimensional failure mechanism over the footing length L and considering the resulting velocity discontinuity surface at the end faces (Fig. 13). Hence, internal energy dissipation within the soil occurs on the cylindrical surface and on the end circular segments. The resulting objective function is expressed as follows (cf. Appendix A for the mathematical derivation):

$$\begin{aligned}\frac{Q_u}{cB} &= \frac{2}{\zeta_0}\mu + \zeta_0 K_{c1} + \zeta_0^2 K_{c2}\frac{B}{L}\\ K_{c1} &= 2\left(\frac{\pi - 2\theta_0}{\cos^2\theta_0} + \beta\tan\theta_0\right)\\ K_{c2} &= \frac{4}{3}\left\{\frac{\pi - 2\theta_0}{\cos^3\theta_0} - \frac{\tan^3\theta_0}{4}\left[\sin^{-2}(\theta_0/2) - \cos^{-2}(\theta_0/2) + 4\ln\frac{\cos(\theta_0/2)}{\sin(\theta_0/2)}\right]\right\}\end{aligned} \tag{25}$$

where $\zeta_0 = x_0/B$. The solution is found through the following bounded optimisation problem:

$$\begin{aligned}&\min_{\zeta_0,\theta_0} \frac{Q_u}{cB}\\ &\zeta_0 > 0\\ &0 < \theta_0 < \pi\end{aligned} \tag{26}$$

which was solved numerically as before. The results for perfectly adherent footings ($\beta = 1$) are plotted for $B/L = 0$, 0.5 and 1 in Fig. 14. To the best of authors' knowledge, the best upper bound for rectangular rigid footings was obtained by Salgado et al. (2004) with the limit analysis and finite element method. For the considered rectangular and square shapes, they obtained $N_c = 6.02$ and 6.22, respectively. For comparison, the complete solution for a perfectly adherent circular punch was obtained by Eason and Shield (1960) and is $N_c = 6.05$. The bearing capacity of a Tresca material increases with increasing aspect ratio B/L owing to the presence of hoop stresses (Hencky, 1923; Meyerhof, 1951). This is also observed in the combined failure. Note that this explanation for enhanced bearing capacity leads to the conclusion that it is maximum for circular footings (Skempton, 1951; Meyerhof, 1963). Thus, it is likely that $N_c = 6.05$ is an absolute upper bound to the bearing capacity of any rectangular indenter.

Rigorous lower bound solutions can be obtained in the same way as

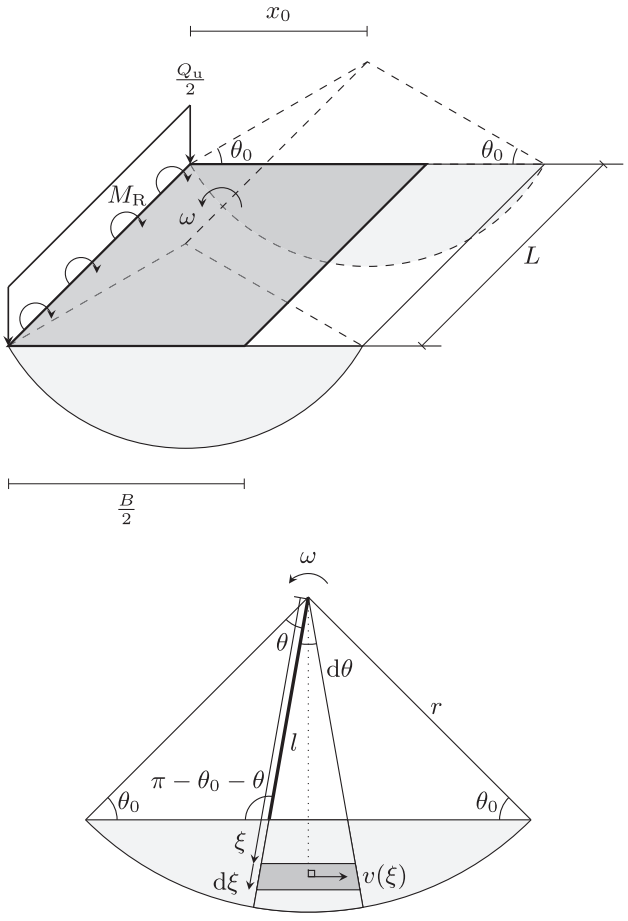

Fig. 13. Combined failure mechanism in three dimensions for a Tresca material.

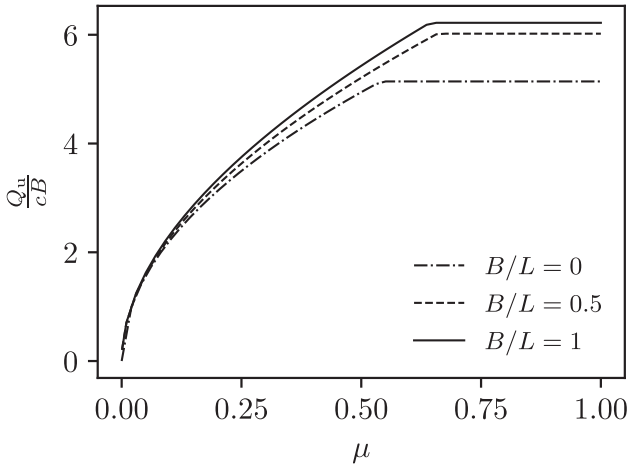

Fig. 14. Upper bounds to the collapse load for perfectly adherent rectangular footings with finite flexural resistance resting on a Tresca half-space.

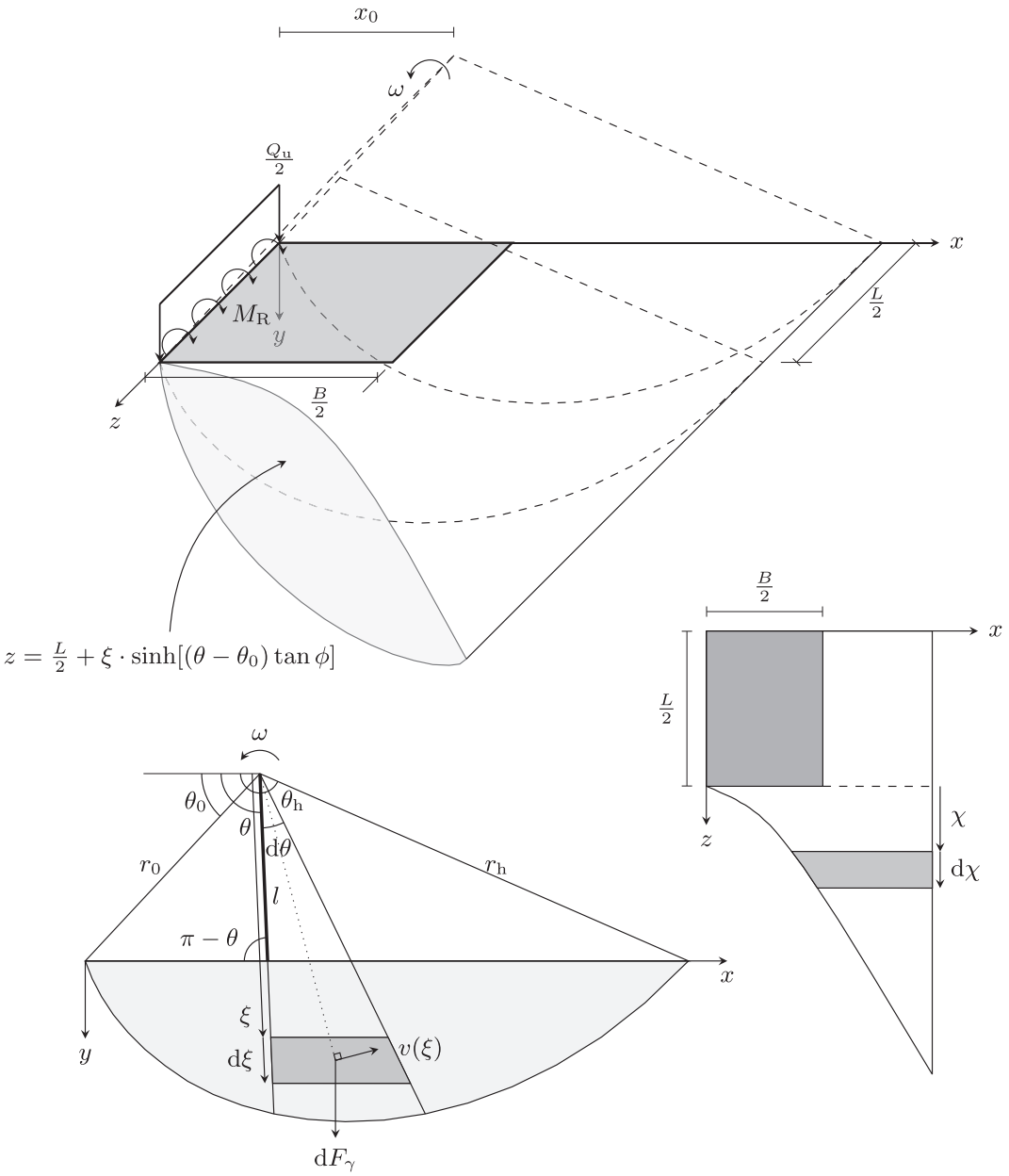

Fig. 15. Combined failure mechanism in three dimensions for a Mohr–Coulomb material.

for strip footings. The pressure distribution is not uniform but increases slightly toward the footing centre. However, given that the bearing pressure increases with B/L, an absolute lower bound may be obtained assuming a uniform pressure distribution equal to $c(2+\pi)$.

The geometry of the end failure surfaces for a Mohr–Coulomb material is more complex because the normality condition imposes an angle ϕ between the velocity vectors and the velocity discontinuity surface. Such a surface for a plane strain motion was derived by Garnier (1995) and is depicted in Fig. 15. The kinematics is similar to the previous cases, with velocity vectors parallel to the *xy*-plane.

The objective function for a cohesionless Mohr–Coulomb soil is expressed as follows (refer to Appendix B for further details regarding its derivation):

$$\frac{2Q_u}{\gamma B^2} = \frac{2}{1-\tan\delta\tan\theta_0}\left(\frac{2}{\zeta_0}\eta + 2K_{\gamma 1}\zeta_0^2 + \frac{B}{L}K_{\gamma 2}\zeta_0^3\right)$$

$$K_{\gamma 1} = -\frac{f_1}{\cos^3\theta_0} + \frac{\tan\theta_0}{6} - \frac{\tan^3\theta_0}{6\tan^2\theta_h} \tag{27}$$

$$K_{\gamma 2} = -\frac{1}{\cos^4\theta_0}\int_{\theta_0}^{\theta_h}\left(e^{4(\theta-\theta_0)\tan\phi} - \frac{\sin^4\theta_0}{\sin^4\theta}\right)\sinh[(\theta-\theta_0)\tan\phi]\cos\theta\,d\theta$$

where f_1 was derived by Chen (1975):

$$f_1 = \frac{1}{3(1+9\tan^2\phi)}\left[(3\tan\phi\cos\theta_h + \sin\theta_h)e^{3(\theta_h-\theta_0)\tan\phi} - 3\tan\phi\cos\phi - \sin\theta_0\right] \tag{28}$$

Given that θ_h and θ_0 are related through the implicit equation $\sin\theta_h\exp[(\theta_h-\theta_0)\tan\phi] - \sin\theta_0 = 0$ (Plumey, 2007), the optimisation problem is expressed as follows:

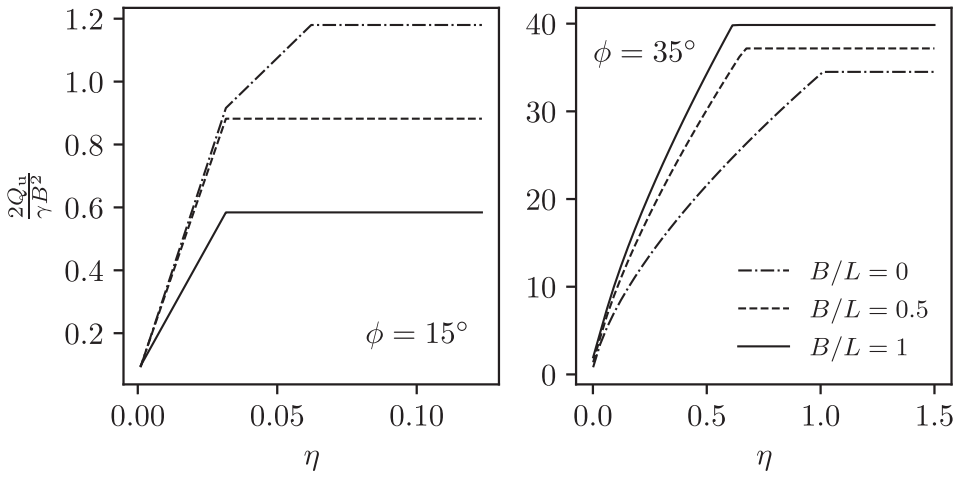

Fig. 16. Upper bounds to the collapse load for perfectly rough ($\delta = \phi$) rectangular footings with finite flexural resistance resting on a cohesionless Mohr–Coulomb half-space.

$$\min_{\zeta_0,\theta_0} \frac{2Q_u}{\gamma B^2}$$
$$\zeta_0 > 0 \tag{29}$$
$$\begin{cases} 0 < \theta_0 < \pi & \text{if } \delta = 0 \\ 0 < \theta_0 < \tan^{-1}(1/\tan\delta) & \text{otherwise} \end{cases}$$

In (27), the integral was numerically evaluated with the scipy.integrate.quad function of SciPy and the optimisation was carried out as in the previous case.

Results for perfectly rough interfaces ($\delta = \phi$), $\phi = 15°$ and $35°$ are given in Fig. 16. The bearing capacity for rectangular rigid footings is computed by multiplying the exact solution for strip footings (Martin, 2005b) with the analytical expression of the shape factor derived by

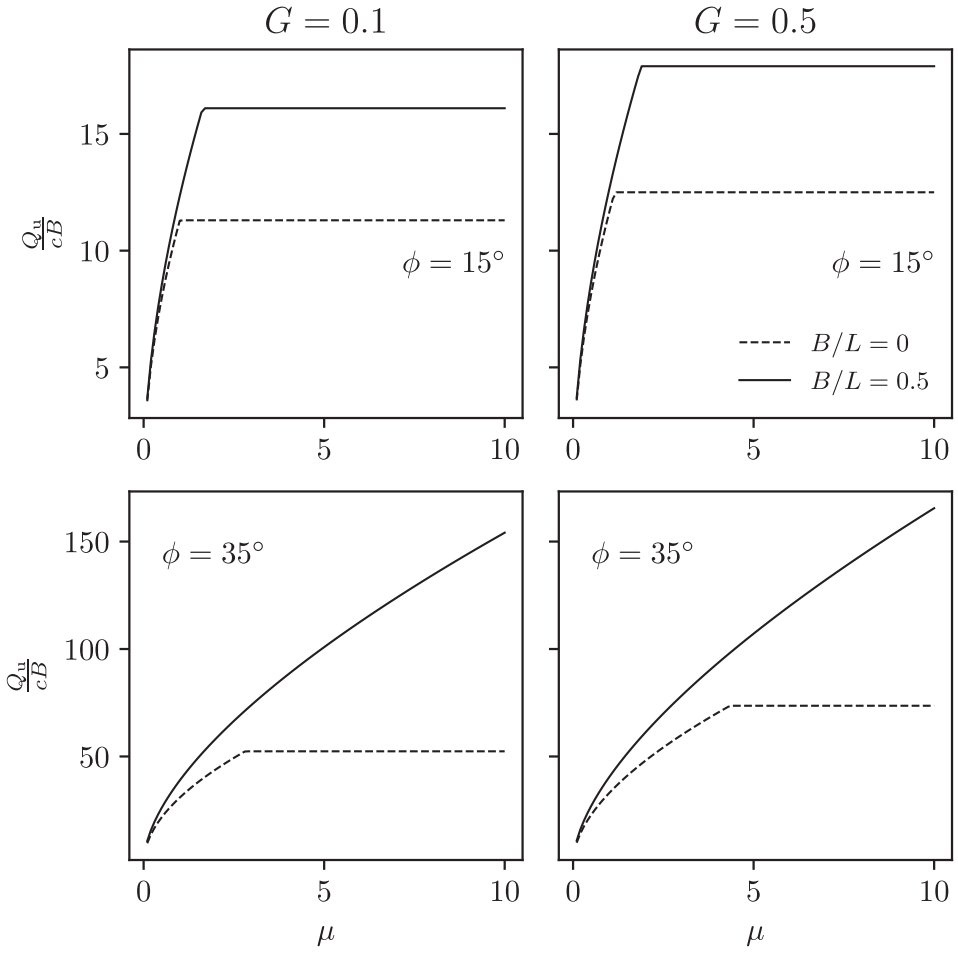

Fig. 17. Upper bounds to the collapse load for perfectly rough ($\delta = \phi$) rectangular footings with finite flexural resistance resting on general Mohr–Coulomb half-spaces.

Lyamin et al. (2007), which is based on a weighted average of lower and upper bounds, and thus it is supposed to provide reasonable estimates of the exact solution. Note that the bearing capacity increases with increasing B/L for $\phi = 35\%$, whereas the situation is reversed for $\phi = 15^\circ$. This seems inconsistent with respect to the experimental results previously mentioned, according to which the bearing capacity decreases with decreasing L. The reason for this is twofold. First, the shear strength angle for conditions other than plane strains is lower (Meyerhof, 1963). Second, finite element simulations showed that, for small values of ϕ, the mass of displaced soil reduces with increasing B/L (Zhu and Michalowski, 2005). This causes a reduction of the bearing capacity. The same was observed for higher values of the shear strength angle and dilatancy angles lower than ϕ, which is generally the case for real soils.

To obtain a lower bound, the same approach of the plane strain problem can be adopted but with extension of the shape of the contact pressure distribution to three dimensions. In particular, the pressure must be zero over the entire perimeter of the footing. This actually produces a movement of the resultant pressure closer to the footing centre.

In the case of general Mohr–Coulomb soils, the contribution of the cohesion to the internal energy dissipation must be added to the previous solution. The objective function can be expressed as follows (cf. Appendix C):

$$\begin{aligned}
&\frac{Q_u}{cB} = \frac{1}{1-\tan\delta\tan\theta_0}\left[\frac{2}{\zeta_0}\mu + K_1\zeta_0 + 4\left(\frac{B}{L}K_2 - GK_3\right)\zeta_0^2 - \frac{B}{L}GK_4\zeta_0^3\right] \\
&K_1 = \frac{e^{2(\theta_h-\theta_0)\tan\phi}-1}{\cos^2\theta_0\tan\phi} \\
&K_2 = \frac{1}{3\cos^3\theta_0}\int_{\theta_0}^{\theta_h}\left(e^{3(\theta-\theta_0)\tan\phi} - \frac{\sin^3\theta_0}{\sin^3\theta}\right)\cosh[(\theta-\theta_0)\tan\phi]\,\mathrm{d}\theta \\
&K_3 = -K_{\gamma 1} \\
&K_4 = -\frac{K_{\gamma 2}}{2}
\end{aligned} \tag{30}$$

with the following optimisation problem:

$$\begin{aligned}
&\min_{\zeta_0,\theta_0}\frac{Q_u}{cB} \\
&\zeta_0 > 0 \\
&\begin{cases} 0 < \theta_0 < \pi & \text{if } \delta = 0 \\ 0 < \theta_0 < \tan^{-1}(1/\tan\delta) & \text{otherwise} \end{cases}
\end{aligned} \tag{31}$$

Results for perfectly rough interfaces, obtained in a similar way to the previous ones for $G = 0.1$ and 0.5, $\phi = 15^\circ$ and 35°, and $B/L = 0$ and 0.5, are plotted in Fig. 17. A few rigorous upper bound solutions are available for the bearing capacity of finite length footings resting on general soils. The reason for this is that an optimum solution exists for any combination of the parameters G, ϕ, and B/L, which complicates to derive useful and simple analytical expressions or charts. Moreover, practitioners prefer the superposition approach owing to its conservative character. The solutions for rigid footings retained here correspond to the upper bounds obtained by Michalowski (2001), who considered an advanced multi-block Prandtl-type failure mechanism. Note that, for the selected values of G, the bearing capacity increases with increasing B/L, similar to the case of a Tresca material. This is due to the fact that, as a rough estimate, a weightless material can be assumed for $G < 0.1$, whereas a cohesionless material can be assumed for $G > 10$ (Chen, 1975). Therefore, the situation is closer to a weightless material.

An absolute lower bound corresponding to a weightless soil and a smooth footing can be obtained with the admissible uniform contact pressure obtained by Shield (1955). Improved solutions require to take into account the soil self-weight and eventually the base roughness. The superposition approach can be adopted, as in the case of strip footings.

4. Concluding remarks

A general framework for the analysis of the bearing capacity of surface footings under centred vertical load considering soil-structure interaction was presented. The importance of considering both components, i.e. the ground and the structure, for a correct evaluation of the overall foundation resistance was emphasised. A simple procedure based on the knowledge of an approximate contact pressure distribution combined with the knowledge of the governing footing failure mode was shown to be a powerful tool for consistent foundation analysis and design.

Detailed analyses of the bearing capacity problem of a surface footing with a very slender cross-section was carried out to show how the limit analysis method can be applied to general three-dimensional soil-structure systems.

The evaluation of the footing bearing capacity assuming a uniform contact pressure distribution, regardless of the soil properties, is only justified for deep beam footings.

Previous studies coincide on the fact that the contact pressure distribution at the instant of general shear failure is closely approximated by one of the following simple shapes: uniform, triangular, ellipsoidal, and trapezoidal. This can be conveniently exploited to take into account the soil-structure interaction in a simplified manner.

The concepts and techniques presented in this paper can be extended to shallow footings subjected to general loading conditions and to other soil-structure systems, such as retaining walls.

Credit authorship contribution statement

Cristiano Garbellini: Conceptualization, Formal analysis, Methodology, Writing. **Lyesse Laloui:** Supervision.

Declaration of Competing Interest

The authors declare that they have no known competing financial interests or personal relationships that could have appeared to influence the work reported in this paper.

Acknowledgements

This study was supported by the Swiss National Science Foundation (financial support No. 200021_175500, Division II).

Appendix A. 3D combined failure mechanism on a Tresca material

The external power resulting from the applied load, the rate of internal energy dissipation due to the plastic hinge, the interface adherence, and the lateral cylindrical surfaces are simply obtained by multiplying the expressions for the plane strain problem (Plumey, 2007) times the footing length L. The expression of interface dissipation is based on the assumption, verified a posteriori, that $\min\{r\cos\theta_0; B/2\} = r\cos\theta_0$.

The rate of energy dissipation due to plastic shearing at the end faces is given by the following expression (cf. Fig. 13):

$$D_{c2} = 4\int_{\theta=0}^{\theta=\pi-2\theta_0}\int_{\xi=l}^{\xi=r}\mathrm{d}D_{c2} \tag{A.1}$$

where $l = r\sin\theta_0/\sin(\theta_0+\theta)$ (thick black line in Fig. 13) and and $\mathrm{d}D_{c2} = cv\mathrm{d}A = c\omega\xi^2\,\mathrm{d}\xi\,\mathrm{d}\theta$ with $\mathrm{d}A$ the differential of the lateral end surface area (dark grey rectangle in Fig. 13). Dissipation D_{c2} is expressed as follows:

$$D_{c2} = \frac{4}{3}c\omega r^3\left(\pi - 2\theta_0 - \sin^3\theta_0\int_{\theta=0}^{\theta=\pi-2\theta_0}\sin^{-3}(\theta_0+\theta)\,\mathrm{d}\theta\right) \tag{A.2}$$

introducing $M_R = \mu cB^2, r = \zeta_0 B/\cos\theta_0$, and knowing that the following expressions are fulfilled:

$$\int_{\theta=0}^{\theta=\pi-2\theta_0}\sin^{-3}(\theta_0+\theta)\,\mathrm{d}\theta = \frac{1}{4}\left[\sin^{-2}(\theta_0/2) - \cos^{-2}(\theta_0/2)\right] + \ln\frac{\cos(\theta_0/2)}{\sin\theta_0/2} \tag{A.3}$$

the objective function (25) is obtained.

Appendix B. 3D combined failure mechanism on a cohesionless Mohr–Coulomb material

As in the case of a Tresca soil, the solution is obtained by multiplying the expressions for the plane strain problem (Plumey, 2007) times L, and by adding the contribution of the end regions. For a cohesionless Mohr–Coulomb material, the latter participates in the external power of the gravity field P_γ. Considering only one quarter of the failure mechanism, the exercise consists in computing the rate of work done by the gravity force in the region $z \geqslant L/2$ (cf. Fig. 15). Considering the bounds of the integration variables:

$$\begin{aligned}&\theta_0 \leqslant \theta \leqslant \theta_h\\ &l(\theta) \leqslant \xi \leqslant r(\theta)\\ &0 \leqslant \chi \leqslant z(\xi,\theta)\end{aligned} \tag{B.1}$$

where

$$\begin{aligned}&l(\theta) = r_0\sin\theta_0/\sin\theta\\ &r(\theta) = r_0 e^{(\theta-\theta_0)\tan\phi}\\ &z(\xi,\theta) = \xi\sinh[(\theta-\theta_0)\tan\phi]\end{aligned} \tag{B.2}$$

P_γ is expressed as follows:

$$\begin{aligned}\frac{P_\gamma}{4} &= \int_{\theta=\theta_0}^{\theta=\theta_h}\int_{\xi=l}^{\xi=r}\int_{\chi=0}^{\chi=z}\mathrm{d}P_\gamma\\ &= \frac{1}{4}\omega\gamma r_0^4\int_{\theta_0}^{\theta_h}\left(e^{4(\theta-\theta_0)\tan\phi} - \frac{\sin^4\theta_0}{\sin^4\theta}\right)\sinh[(\theta-\theta_0)\tan\phi]\cos\theta\,\mathrm{d}\theta\end{aligned} \tag{B.3}$$

where the differential of the rate of gravitational work is $\mathrm{d}P_\gamma = \gamma\omega\xi^2\cos\theta\,\mathrm{d}\chi\,\mathrm{d}\xi\,\mathrm{d}\theta$. Finally, the objective function (27) is obtained by considering that $r_0 = \zeta_0 B/\cos\theta_0$ and $M_R = \eta\gamma B^3$.

Appendix C. 3D combined failure mechanism on a Mohr–Coulomb material

The upper bound solution for the combined three-dimensional failure mechanism and a general Mohr–Coulomb soil is obtained from the plane strain solution (Garbellini and Laloui, 2018) and the three-dimensional solution for the cohesionless soil (Appendix B). The former is extended over the entire footing length. The formulation of the rate of work due to the gravity force for the end regions of the latter remains the same, and the contribution of the apparent cohesion to the internal energy dissipation D_c on the end faces is added.

Given that velocity vectors make an angle ϕ with the discontinuity surface, the differential of energy dissipation is $\mathrm{d}D_c = c\omega r\cos\phi\,\mathrm{d}A$, where the differential of surface area in cylindrical coordinates is expressed as follows:

$$\begin{aligned}&\mathrm{d}A = \sqrt{1+\left(\frac{\partial z}{\partial\xi}\right)^2 + \frac{1}{\xi^2}\left(\frac{\partial z}{\partial\theta}\right)^2}\;\xi\,\mathrm{d}\xi\,\mathrm{d}\theta\\ &\frac{\partial z}{\partial\xi} = \sinh[(\theta-\theta_0)\tan\phi]\\ &\frac{\partial z}{\partial\theta} = \xi\cosh[(\theta-\theta_0)\tan\phi]\tan\phi\end{aligned} \tag{C.1}$$

Considering the integration variables θ and ξ as in Eq. (B.1), the contribution of the cohesion is given by the following expression:

$$\begin{aligned}\frac{D_c}{4} &= c\omega\cos\phi\int_{\theta=\theta_0}^{\theta=\theta_h}\int_{\xi=l}^{\xi=r}\sqrt{\cosh^2[(\theta-\theta_0)\tan\phi]\left(1+\tan^2\phi\right)}\;\xi^2\,\mathrm{d}\xi\,\mathrm{d}\theta\\ &= c\omega\frac{r_0^3}{3}\int_{\theta=\theta_0}^{\theta=\theta_h}\left(e^{3(\theta-\theta_0)\tan\phi} - \frac{\sin^3\theta_0}{\sin^3\theta}\right)\cosh[(\theta-\theta_0)\tan\phi]\,\mathrm{d}\theta\end{aligned} \tag{C.2}$$

Finally, by applying the principle of virtual velocities, rearranging the terms, and considering that $r_0 = \zeta_0 B/\cos\theta_0, M_R = \mu cB^2$, and $G = 0.5\gamma B/c$,

Eq. (30) is recovered.

References

Bazant, Z.P., Kim, J.K., 1984. Size effect in shear failure of longitudinally reinforced beams. American Concrete Institute.

Bolton, M.D., Lau, C.K., 1993. Vertical bearing capacity factors for circular and strip footings on mohr–coulomb soil. Can. Geotech. J. 30, 1024–1033.

Byrd, R.H., Lu, P., Nocedal, J., Zhu, C., 1995. A limited memory algorithm for bound constrained optimization. SIAM J. Sci. Comput. 16, 1190–1208.

Campana, S., Fernández Ruiz, M., Muttoni, A., 2014. Strength of arch-shaped members in bending and shear. In: 4th fib Congress, Mumbai, 4th fib Congress, Mumbai. p. 9.

Campana, S., Muttoni, A., 2010. Analysis and design of an innovative solution for tunnels using elastic-plastic stress fields. In: Proceeding of the 8th fib-PhD Symposium, Proceeding of the 8th fib-PhD Symposium. pp. 75–80.

Cavagnis, F., 2017. Shear in reinforced concrete without transverse reinforcement.

Cavagnis, F., Fernández Ruiz, M., Muttoni, A., 2015. Shear failures in reinforced concrete members without transverse reinforcement: An analysis of the critical shear crack development on the basis of test results. Eng. Struct. 103, 157–173.

Cavagnis, F., Fernández Ruiz, M., Muttoni, A., 2018. A mechanical model for failures in shear of members without transverse reinforcement based on development of a critical shear crack. Eng. Struct. 157, 300–315.

Chen, W.F., 1975. Limit Analysis and Soil Plasticity, first ed. Elsevier.

Cox, A.D., 1962. Axially-symmetric plastic deformation in soils–ii. Indentation of ponderable soils. Int. J. Mech. Sci. 4, 371–380.

Davis, E.H., Booker, J.R., 1971. The bearing capacity of strip footings from the standpoint of plasticity theory. In: Proc. 1st Australia-New Zeland Conf. on Proc. 1st Australia-New Zeland Conf. on Geomechanics, Melbourne, Australia, pp. 276–282.

Davis, E.H., Booker, J.R., 1973. The effect of increasing strength with depth on the bearing capacity of clays. Geotechnique 23, 551–563.

Davis, R.O., Selvadurai, A.P.S., 1996. Elasticity and Geomechanics, 201 pages. University Press, Cambridge.

de Beer, E.E., 1961. Etude expérimentale de la capacité portante du sable sous des fondations circulaires établies en surface. In: Proc. 5th Int. Conf. on SMFE, pp. 577–581.

de Beer, E.E., 1970. Experimental determination of the shape factors and the bearing capacity factors of sand. Geotechnique 20, 387–411.

de Buhan, P., 2007. Plasticité et calcul à la rupture. Presses des Ponts.

Drescher, A., Detournay, E., 1993. Limit load in translational failure mechanisms for associative and non-associative materials. Géotechnique 43, 443–456.

Drucker, D.C., 1953. Coulomb friction, plasticity, and limit loads. Technical Report. Brown Univ Providence Ri Div of Applied Mathematics.

Drucker, D.C., Greenberg, H.J., Prager, W., 1951. The safety factor of an elastic-plastic body in plane strain. J. Appl. Mech. 18, 371–378.

Drucker, D.C., Prager, W., 1952. Soil mechanics and plastic analysis or limit design. Quart. Appl. Math. 10, 157–165.

Drucker, D.C., Prager, W., Greenberg, H.J., 1952. Extended limit design theorems for continuous media. Quart. Appl. Math. 9, 381–389.

Eason, G., Shield, R.T., 1960. The plastic indentation of a semi-infinite solid by a perfectly rough circular punch. Zeitschrift für angewandte Mathematik und Physik ZAMP 11, 33–43.

Fernández Ruiz, M., Muttoni, A., 2007. On development of suitable stress fields for structural concrete. ACI, Struct. J. 104, 495–502.

Fernández Ruiz, M., Muttoni, A., Sagaseta, J., 2015. Shear strength of concrete members without transverse reinforcement: A mechanical approach to consistently account for size and strain effects. Eng. Struct. 99, 360–372.

Garbellini, C., Laloui, L., 2018. On the soil-structure interaction of surface strip footings at ultimate limit state, in. In: 26th European Young Geotechnical Engineers Conference, ISSMGE.

Garnier, D., 1995. Analyse par la théorie du calcul à la rupture des facteurs de réduction de la capacité portante de fondations superficielles. Ph.D. thesis.

Golder, H.Q., 1942. The ultimate bearing pressure of rectangular footings. J. Inst. Civil Eng. 18, 161–174.

Gourvenec, S., Randolph, M.F., Kingsnorth, O., 2006. Undrained bearing capacity of square and rectangular footings. Int. J. Geomech. 6, 147–157.

Hansen, B., 1961. The bearing capacity of sand, tested by loading circular plates. In: 5th International Conference on Soil Mechanic Foundation, England, pp. 659–664.

Hencky, H., 1923. Über einige statisch bestimmte fälle des gleichgewichts in plastischen körpern. ZAMM-J. Appl. Math. Mech./Zeitschrift für Angewandte Mathematik und Mechanik 3, 241–251.

Hill, R., 1951. On the state of stress in a plastic-rigid body at the yield point. London, Edinburgh, Dublin Philos. Mag. J. Sci. 42, 868–875.

Kani, G.N.J., 1964. The riddle of shear failure and its solution. J. Proc. 441–468.

Kostic, N., 2009. Topologie des champs de contraintes pour le dimensionnement des structures en béton armé.

Kumar, J., 2003. $N_\gamma$for rough strip footing using the method of characteristics. Can. Geotech. J. 40, 669–674.

Larkin, L.A., 1968. Theoretical bearing capacity of very shallow footings. J. Soil Mech. Found. Div. 94, 1347–1360.

Limit State Ltd., 2019. Limit state. http://limitstate.com/.

Loukidis, D., Chakraborty, T., Salgado, R., 2008. Bearing capacity of strip footings on purely frictional soil under eccentric and inclined loads. Can. Geotech. J. 45, 768–787.

Loukidis, D., Salgado, R., 2009. Bearing capacity of strip and circular footings in sand using finite elements. Comput. Geotech. 36, 871–879.

Lundgren, H., Mortensen, K., 1953. Determination by the theory of plasticity of the bearing capacity of continuous footings on sand. In: Proc., 3th Int. Conf. Soil Mech. Found. Eng, pp. 409–412.

Lyamin, A.V., Salgado, R., Sloan, S.W., Prezzi, M., 2007. Two-and three-dimensional bearing capacity of footings in sand. Géotechnique 57, 647–662.

Marti, P., 1985. Basic tools of reinforced concrete beam design. J. Proc. 46–56.

Martin, C.M., 2004. ABC–analysis of bearing capacity. Available online from http://www2.eng.ox.ac.uk/civil/people/cmm/software.

Martin, C.M., 2005a. Exact bearing capacity calculations using the method of characteristics. Proc. IACMAG. Turin 441–450.

Martin, C.M., 2005b. Exact bearing capacity factors for strip footings–notes. Available online from http://www2.eng.ox.ac.uk/civil/people/cmm.

Meyerhof, G.G., 1948. An investigation of the bearing capacity of shallow footings on dry sand. In: Proc. 2nd ICSMFE, pp. 238–243.

Meyerhof, G.G., 1951. The ultimate bearing capacity of foudations. Geotechnique 2, 301–332.

Meyerhof, G.G., 1955. Influence of roughness of base and ground-water conditions on the ultimate bearing capacity of foundations. Geotechnique 5, 227–242.

Meyerhof, G.G., 1961. Discussion on foundations other than piled foundations, in. In: Proceedings, 5th International Conference on Soil Mechanics and Foundation Engineering, Paris, pp. 193–195.

Meyerhof, G.G., 1963. Some recent foundation research and its application to design. Struct. Eng. 31, 151–167.

Michalowski, R.L., 1997. An estimate of the influence of soil weight on bearing capacity using limit analysis. Soils Found. 37, 57–64.

Michalowski, R.L., 2001. Upper-bound load estimates on square and rectangular footings. Géotechnique 51, 787–798.

Michalowski, R.L., Dawson, E.M., 2002. Three-dimensional analysis of limit loads on mohr-coulomb soil. Found. Civil Environ. Eng. 1, 137–147.

Muttoni, A., Fernández Ruiz, M., 2008a. Shear strength in one-and two-way slabs according to the critical shear crack theory. In: fib Symposium, Amsterdam 2008, fib Symposium, Amsterdam 2008.

Muttoni, A., Fernández Ruiz, M., 2008. Shear strength of members without transverse reinforcement as function of critical shear crack width. ACI Struct. J. 2, 163–172.

Muttoni, A., Fernández Ruiz, M., Kostic, N., 2011. Champs de contraintes et méthode des bielles-et-tirants–Applications dans la conception et le dimensionnement des structures en béton armé. Technical Report. EPFL-IBETON.

Muttoni, A., Fernández Ruiz, M., Simões, J.T., 2018. The theoretical principles of the critical shear crack theory for punching shear failures and derivation of consistent closed-form design expressions. Struct. Concrete 19, 174–190.

Muttoni, A., Schwartz, J., 1991. Behavior of beams and punching in slabs without shear reinforcement. In: IABSE colloquium, IABSE Colloquium., pp. 703–708.

Muttoni, A., Schwartz, J., Thürlimann, B., 1996. Design of Concrete Structures with Stress Fields. Springer Science & Business Media.

Optum Computational Engineering, 2019. OptumCE. https://optumce.com/.

Pérez Caldentey, A., Padilla, P., Muttoni, A., Fernández Ruiz, M., 2012. Effect of load distribution and variable depth on shear resistance of slender beams without stirrups. ACI Struct. J. 109, 595–603.

Plumey, S., 2007. Interaction sol-structure dans le domaine des tranchées couvertes. Ph. D. thesis. École polytechnique eédérale de Lausanne.

Plumey, S., Muttoni, A., Vulliet, L., Labiouse, V., 2004. Plasticity in soil-structure interaction applied to cut-and-cover tunnels. In: 5th International PhD Symposium in Civil Engineering, 5th International PhD Symposium in Civil Engineering, pp. 989–995.

Prandtl, L., 1920. Über die härte plastischer körper. Nachrichten von der Gesellschaft der Wissenschaften zu Göttingen, Mathematisch-Physikalische Klasse 1920, 74–85.

Rankine, W.J.M., 1857. On the stability of loose earth. Philos. Trans. Roy. Soc. London 9–27.

Salgado, R., Lyamin, A.V., Sloan, S.W., Yu, H.S., 2004. Two-and three-dimensional bearing capacity of foundations in clay. Géotechnique 54, 297–306.

Saran, S., 2017. Shallow Foundations and Soil Constitutive Laws. CRC Press.

Schlaich, J., Schäfer, K., Jennewein, M., 1987. Toward a consistent design of structural concrete. PCI J. 32, 74–150.

Shield, R.T., 1955. On coulomb's law of failure in soils. J. Mech. Phys. Solids 4, 10–16.

Shield, R.T., 1955. On the plastic flow of metals under conditions of axial symmetry. Proc. Roy. Soc. London. Ser. A. Math. Phys. Sci. 233, 267–287.

Shield, R.T., Drucker, D.C., 1953. The application of limit analysis to punch-indentation problems. J. Appl. Mech. 453–460.

SIA, 2013. Code 262 for Concrete Structures. Swiss Society of Engineers and Architects, Zurich, Switzerland, p. 2013.

Simões, J.T., Bujnak, J., Fernández Ruiz, M., Muttoni, A., 2016. Punching shear tests on compact footings with uniform soil pressure. Struct. Concrete 17, 603–617.

Simões, J.T., Faria, D.M.V., Fernández Ruiz, M., Muttoni, A., 2016. Strength of reinforced concrete footings without transverse reinforcement according to limit analysis. Eng. Struct. 112, 146–161.

Skempton, A.W., 1942. An investigation of the bearing capacity of a soft clay soil. J. Inst. Civil Eng. 18, 307–321.

Skempton, A.W., 1951. The bearing capacity of clays. In: Proceedings Building Research Congress, pp. 180–189.

Smith, C.C., 2005. Complete limiting stress solutions for the bearing capacity of strip footings on a mohr-coulomb soil. Géotechnique 55, 607–612.
Stefanou, G.D., 1983. Shear resistance of reinforced concrete beams with non-prismatic sections. Eng. Fract. Mech. 18, 643–666.
Taylor, D.W., 1948. Fundamentals of Soil Mechanics. vol. 66. LWW.
Terzaghi, K., 1943. Theoretical Soil Mechanics. Wiley.
Vecchio, F.J., Collins, M.P., 1986. The modified compression-field theory for reinforced concrete elements subjected to shear. ACI J. 83, 219–231.
Virtanen, P., Gommers, R., Oliphant, T.E., Haberland, M., Reddy, T., Cournapeau, D., Burovski, E., Peterson, P., Weckesser, W., Bright, J., Van der Walt, S.J., Brett, M., Wilson, J., Jarrod Millman, K., Mayorov, N., Nelson, A.R.J., Jones, E., Kern, R., Larson, E., Carey, C.J., Polat, I., Feng, Y., Moore, E.W., Vand erPlas, J., Laxalde, D., Perktold, J., Cimrman, R., Henriksen, I., Quintero, E.A., Harris, C.R., Archibald, A. M., Ribeiro, A.H., Pedregosa, F., Van Mulbregt, P., Contributors, S., et al., 2020. Scipy 1.0: Fundamental algorithms for scientific computing in python. Nat. Methods 17, 261–272. https://doi.org/10.1038/s41592-019-0686-2.
Zhu, M., Michalowski, R.L., 2005. Shape factors for limit loads on square and rectangular footings. J. Geotech. Geoenviron. Eng. 131, 223–231.